Inorganic Chemistry

pubs.acs.org/IC Article

Aggregation versus Biological Activity in Gold(I) Complexes. An Unexplored Concept

Andrea Pinto,[†] Catarina Roma-Rodrigues,[†] Jas S. Ward, Rakesh Puttreddy, Kari Rissanen, Pedro V. Baptista, Alexandra R. Fernandes,* João Carlos Lima, and Laura Rodríguez*

Cite This: https://doi.org/10.1021/acs.inorgchem.1c02359 Read Online

ACCESS | Metrics & More | Article Recommendations | Supporting Information

ABSTRACT: The aggregation process of a series of mono- and dinuclear gold(I) complexes containing a 4-ethynylaniline ligand and a phosphane at the second coordination position (PR_3-Au-C≡CC_6H_4-NH_2, complexes **1**−**5**, and (diphos)(Au-C≡CC_6H_4-$NH_2)_2$, complexes **6**−**8**), whose biological activity was previously studied by us, has been carefully analyzed through absorption, emission, and NMR spectroscopy, together with dynamic light scattering and small-angle X-ray scattering. These experiments allow us to retrieve information about how the compounds enter the cells. It was observed that all compounds present aggregation in fresh solutions, before biological treatment, and thus they must be entering the cells as aggregates. Inductively coupled plasma atomic emission spectrometry measurements showed that mononuclear complexes are mainly found in the cytosolic fraction; the dinuclear complexes are mainly found in a subsequent fraction composed of nuclei and cytoskeleton. Additionally, dinuclear complex **8** affects the actin aggregation to a larger extent, suggesting a cooperative effect of dinuclear compounds.

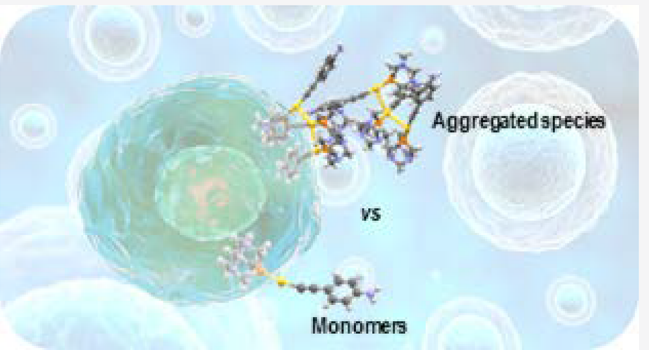

INTRODUCTION

Gold compounds have a long and important tradition from ancient times, where they were already used in medicine (the so-called Chrysotherapy).[1] At the beginning, gold complexes were widely used for the treatment of several diseases, especially as antiinfectious and antitubercular agents, but the treatment of rheumatoid arthritis with a phosphine−gold thiolate complex, auranofin, was a key point in revealing the potential of these types of complexes as metallodrugs. Nowadays, these types of complexes are very well studied because of their potential applications as anticancer agents[2−10] and even, very recently, because of preliminary promising results in the fight against the SARS-CoV2 virus.[11,12] Interestingly, gold(I) metallodrugs display better tolerance in *in vivo* studies than platinum derivatives, which are well-known as anticancer agents since the discover of cisplatinum. Phosphane−gold(I) alkynyl complexes are among the most studied of the gold(I) complexes reported, with some promising results in the literature for potential anticancer activity.[9,13−20]

The mechanism of action of gold(I) complexes seems to be significantly different from that followed by platinum drugs because gold(I) targets cellular enzymes, while platinum compounds target DNA. Knowledge of the interactions of medicinal gold compounds with proteins is highly relevant to understanding and defining their mechanism of action. Proteomic and metallomic strategies were successfully implemented for elucidation of the specific mechanistic features of anticancer metallodrugs uncovering their physiological processes and molecular targets from the perspective of a biological system,[21−23] together with specific techniques including fluorescence spectroscopy and microscopy, X-ray fluorescence spectrometry (total reflection X-ray fluorescence), mass spectrometry, absorption spectroscopy, X-ray crystallography, NMR spectroscopy, X-ray absorption spectroscopy, inductively coupled plasma, and others.[13,19,21,24,25] These studies allowed the determination of local metallic structures participating in the interaction with proteins, speciation of the complexes, cellular uptake, and biodistribution. Interestingly, it seems that the binding of metal complexes to proteins might not alter the protein conformation and the secondary or tertiary structure of the proteins, with metal binding being assured by the directional interactions of the metal with specific residue side chains.[26]

Received: August 3, 2021

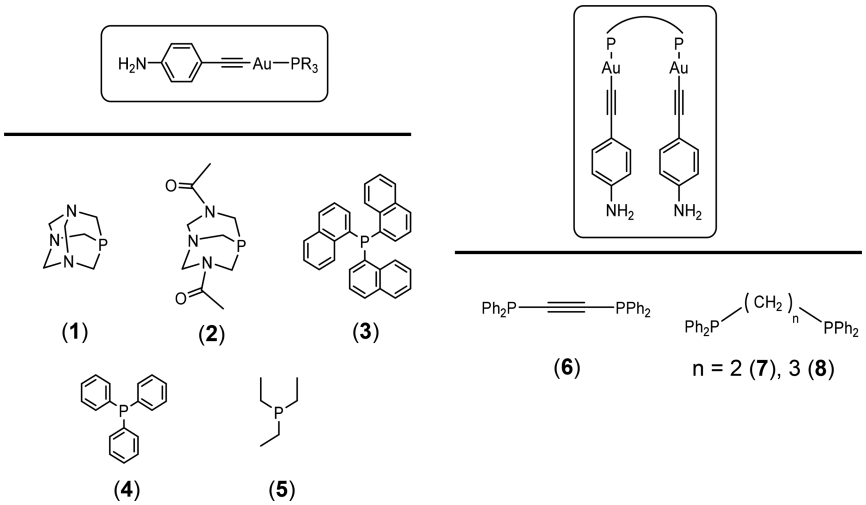

Figure 1. Chemical structures of the biologically active gold(I) complexes studied in this work.

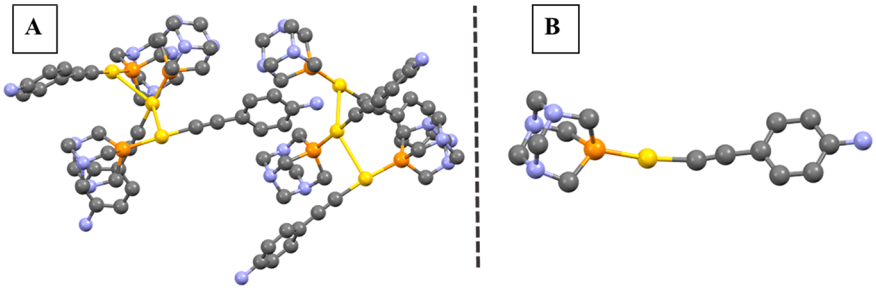

Figure 2. X-ray crystal structures of **1a** (A) and **1b** (B). Color code: yellow, gold; orange, phosphorus; black, carbon; light blue, nitrogen. Hydrogen atoms and solvates have been omitted for clarity.

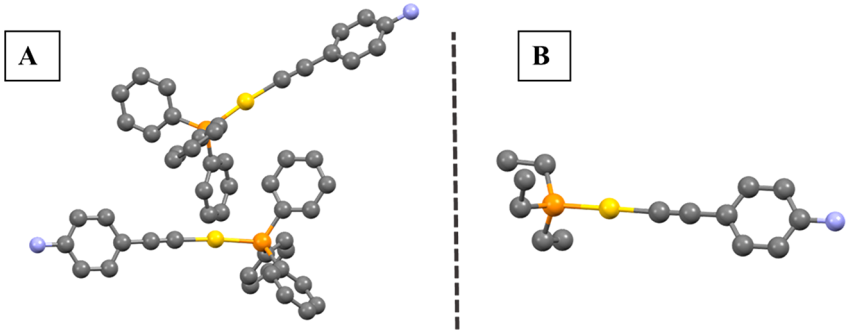

Figure 3. X-ray crystal structures of **4** (A) and **5** (B). Color code: yellow, gold; orange, phosphorus; black, carbon; light blue, nitrogen. Hydrogen atoms have been omitted for clarity.

In general, it is well accepted that the thioredoxin reductase enzyme appears as the main target of these types of metallodrugs because of the high affinity of gold for thiol and selenol groups,[5,7] although their mechanism of action is not completely understood yet, and other targets such as aquaporin-3,[27] zinc finger proteins [such as poly-(adenosnediphosphate riose)polymerase-1],[28] quadruplex DNA,[29,30] and other thiolate-dependent enzymes (such as human glutathione reductase, glutathione peroxidase, glutathione-S-transferases, and cysteine protease)[7] cannot be ignored.

On the other hand, it must be highlighted that gold(I) complexes are well-known to establish gold(I)···gold(I) interactions (either intra- or intermolecularly)[31,32] to yield supramolecular assemblies, which are particularly favored in aqueous solutions even at very dilute concentrations.[33−39] This fact indicated that aggregation might be directly involved in the biological mechanism of gold(I) metallodrugs and that they may be directly administered as aggregates to the cells. Although some studies regarding this field have been found in the literature related to other anticancer drugs with purely organic structures or with nanoparticles,[40,41] to the best of our knowledge, this analysis has no precedent in the literature with metallodrugs [and, in particular, gold(I) metallodrugs] and is also of great relevance toward ongoing drug design.

For this reason, we have synthesized and studied a series of phosphane−gold(I) 4-ethynylaniline complexes whose biological activity was previously reported by us.[13] In this work, careful focus has been put on analysis of the behavior of the metallodrugs before they enter the cells, i.e., how the molecules

https://doi.org/10.1021/acs.inorgchem.1c02359
Inorg. Chem. XXXX, XXX, XXX−XXX

enter the cells and a detailed and complete analysis of their aggregation, in order to retrieve information that should significantly contribute toward the future development and understanding of gold(I) metallodrugs.

RESULTS AND DISCUSSION

Synthesis of the compounds (Figure 1) was performed following the same procedure previously described by us.[13] As in previously explored work, gold(I) alkynyl complexes are well-known to aggregate, both in the solid state and in solution, giving rise to different supramolecular assemblies.[33,35,37,39,42−44] Nevertheless, to the best of our knowledge, the possible correlation between the formation of supramolecular assemblies and the observed biological activity has not yet been explored and was the goal of the studies presented herein.

Aggregation of the Molecules. Single crystals suitable for X-ray diffraction were obtained from dichloromethane/hexane solutions of **1**, **4**, and **5** (Figures 2 and 3). All complexes present a linear coordination around the gold(I) center, with the P−Au−C angles ranging between 169.2(4) and 177.6(1)° (Table 1). The P−Au and Au−C bond distances are in good agreement with those previously reported for gold(I) complexes with the general structure phosphane−gold alkynyl.[13,44−47] The three complexes display near-linear geometry of the P−Au−C≡C−C units and N−H···C_{sp} and C−H···π interactions in the 3D crystal packing, both previously reported in the literature,[13,31,36,48−51] together with aurophilic contacts in both **1a** and **1b**.

Table 1. Selected Bond Lengths (Å) and Angles (deg) for 1, 4, and 5

compound	distance (Å)	angle (deg)
1a	Au−P: 2.257(7)−2.276(8)	P−Au−C: 173.9(8)−177.4(9)
	Au−C: 1.98(3)−2.05(3)	
	Au···Au: 3.083(2)−3.196(2)	
1b	Au−P: 2.256(3)	P−Au−C: 169.2(4)
	Au−C: 2.02(1)	
	Au···Au: 3.444(1)	
4	Au−P: 2.270(1)/2.277(1)	P−Au−C: 173.7(2)/175.0(2)
	Au−C: 1.995(6)/1.996(6)	
	Au···Au: 7.2276(6)	
5	Au−P: 2.280(1)	P−Au−C: 177.6(1)
	Au−C: 2.010(4)	
	Au···Au: 5.1661(4)	

Complex **1** crystallizes in two different solid-state structures, giving colorless and yellow crystals, both of them establishing intermolecular aurophilic contacts. The asymmetric unit of the colorless crystals (**1a**) displays two trimers and two molecules of dichoromethane, and the molecules are twisted in antiparallel conformations connected through aurophilic intermolecular interactions of 3.083(2)−3.196(2) Å, as observed for other previously reported gold(I) complexes (bearing the same phosphane).[35,38] On the other hand, the unit cell of the yellow crystals (**1b**) consists of discrete molecules that are connected through aurophilic contacts of 3.444(1) Å in the 3D crystal packing (Figures 1 and S1 and S2). The asymmetric unit cell of complex **4** contains two molecules in an antiparallel disposition (Figure 3A), while complex **5** crystallizes as a discrete molecule (Figure 3B).

Thus, taking into consideration that the X-ray crystal structures of complexes **3**, **7**, and **8** were also reported in our previous work,[13] the only missing solid-state information is that corresponding to complexes **2** and **6**. Inclusion of the new X-crystal data is of great relevance to support the presence of supramolecular assemblies in all cases in the solid state. Nevertheless, more studies were needed in order to find out if these assemblies persisted in solution, as esd expected for these types of complexes based on previous data.[33] Thus, great effort was put into this work in order to retrieve some information about possible aggregation of the molecules in solution. This will shed some light about the state of the active complexes being of great relevance for the design of new metallodrugs with improved activity in their aggregated forms.

The aggregation process starts at the critical aggregation concentration (c.a.c.), and thus this is a key parameter to be determined. This concentration may depend on several factors, such as the interaction between the complex and solvent (which will depend on the solvent polarity), as well as the bulkiness of the phosphane and/or nuclearity of the complex. In this work, the phosphine bulkiness, hydrophobicity, and nuclearity were modified, while keeping constant all of the other parameters, including the medium, for the purpose of drawing better comparisons. Thus, the absorption and emission spectra at different concentrations were recorded in water/dimethyl sulfoxide (DMSO) mixtures. The plot of the absorption or emission maxima versus concentration enabled determination of the c.a.c. value at the inflection point (Table 2 and Figures S5−S20). It can be observed that all complexes tend to aggregate between 5×10^{-6} and 1×10^{-5} M, where an increase of the baseline is observed because of the dispersion effect of the aggregates,[37] and a new absorption band around 350−400 nm can also be detected in some cases. This new band may be correlated with the formation of aggregates with possible aurophilic contacts.[52] A second emission band also appears at longer wavelengths, around 470 nm, due to the aggregated species. Thus, the bulkiness of the phosphane does not seem to be a key parameter in the aggregation process. In fact, the solubility appeared to be the driving force of this process, with the lowest c.a.c. values in this medium determined for the more insoluble tris(naphthyl)- and diphenylphosphaneacetylene phosphanes.

Table 2. Values of the c.a.c. of Complexes 1−8

compound	c.a.c. (M)	compound	c.a.c. (M)
1	5×10^{-6}	**5**	5×10^{-6}
2	5×10^{-6}	**6**	1×10^{-5}
3	1×10^{-5}	**7**	5×10^{-6}
4	5×10^{-6}	**8**	5×10^{-6}

As expected, emission of the aggregates is affected by the temperature (Figures S21−S25). It can be seen that the aggregation process is more favored at higher temperatures, and it can be assumed that hydrogen-bonding interactions between the complexes and solvent molecules are broken with temperature, thereby favoring hydrophobic interactions, as previously observed for other gold(I) supramolecular assemblies.[34]

The ^{1}H and ^{31}P NMR spectra were performed at different concentrations in water/DMSO mixtures in order to obtain additional information regarding which part of the molecule is more affected during the aggregation process (Figures S26−

https://doi.org/10.1021/acs.inorgchem.1c02359
Inorg. Chem. XXXX, XXX, XXX−XXX

S36). This mixture of solvents was chosen to best approximate the biological experimental conditions. The required concentrations for NMR experiments are higher than those previously used in the absorption and emission experiments, and thus they are all above the c.a.c. The ^{1}H NMR spectra in DMSO-d_6 were also included for those complexes that present lower solubility, which hinders identification of the different peaks in the NMR of the aggregates (see the Supporting Information). Small peaks can be detected close to the main peaks in all cases because of the presence of different types of aggregated species.[34] Additionally, it can be observed that the signals become broader in the presence of deuterated water (D_2O) because of the more favored resulting supramolecular assemblies. Particularly relevant is the case of the more hydrophobic compounds **3** and **6**, where only the peaks of the aniline can be clearly detected. Nevertheless, the corresponding spectrum in pure DMSO-d_6 indicates correct formation of the compounds. It can be observed that for those compounds that contain a more water-soluble phosphane (compounds **1** and **2** with PTA and DAPTA phosphanes, respectively) a slight (0.12 ppm) upfield shift in the phosphane protons, together with the presence of a secondary set of signals related to the aniline moiety, is recorded in the ^{1}H NMR spectra. A slight downfield shift in the ^{31}P NMR spectra (ca. 1.5 ppm) is also observed. This behavior agrees with the presence of larger aggregated assemblies at higher concentrations, where both parts of the molecule (phosphane and aniline group) are affected. This was previously displayed in the X-ray crystal structures because the aurophilic contacts (close to the phosphorus atom) and N−H···π interactions were involved in the intermolecular contacts, affecting their NMR chemical shifts. On the other hand, only the aniline protons are affected by the concentration in the more hydrophobic compounds (i.e., compounds **3** and **5**−**8**) that also display N−H···π interactions in the X-ray crystal structures. Their lower solubility in the experimental conditions supports the formation of more stable aggregates at the lower NMR concentrations used, which is not affected by the further increasing concentrations. A particular case is compound **4**, which contains the triphenylphosphane group, PPh_3, where again both parts of the molecule (aniline and phosphane) are affected by the concentration. The X-ray crystal structure of **4** (Figure S3) shows the presence of intermolecular contacts between the phenyl groups (C−H···π), which may be maintained in solution (in the aggregated form) and can explain the involvement of phosphane in this process, together with the N−H···π interactions involving the aniline.

Correlation between Aggregation and Cell Penetration. The partition coefficients of the compounds were retrieved through absorption spectroscopy in water/octanol mixtures, although the determination of this parameter was only for complexes that possessed at least partial solubility in octanol (compounds **3**−**5** and **8**; Table 3). The observed trend was **8** > **4** > **3** > **5**. The log K_{ow} values are related to the corresponding hydrophobicity of the complexes, and consequently it is expected that the compounds that possess extended aromaticity or a rigid phosphane (and therefore being less soluble in water) might cross the membranes more easily.

The observed aggregation of all of the studied complexes led to an important question regarding the state of the samples in the previously studied biological activity. To understand whether the presence of aggregates plays an important role in the previously studied biological activity of the compounds, several factors were taken into consideration. The first factor considered was the molecules' behavior in aqueous solutions and their uptake by the cells, either as monomers or as aggregates. To shed some light on this issue, absorption spectroscopy and dynamic light scattering (DLS) experiments were recorded at different times (points crucial for the biological assays) and with the same conditions (water solutions with 0.1% DMSO at 37 °C). In all cases, the concentrations used were above the c.a.c. values to favor the formation of aggregates. A decrease in the absorption band is observed at longer times, together with an increase of the baseline due to an increase of the formation of aggregates (Figures S37−S44). Additionally, DLS data revealed that fresh solutions, considered to be t = 0 (recently dissolved molecules), already possess the molecules in their aggregated forms (Figures S45−S52), being a clear indication of the fast kinetic formation of self-assembled structures. Additionally, the recorded sizes at t = 3−6 h are almost constant, which suggests that the fast formation of aggregates is in equilibrium with larger or smaller adducts that are finally thermodynamically stable after this period. Similar experiments carried out in biological media (phosphate-buffered saline) show that, in this medium, aggregation is still present, although smaller sizes can be detected in all cases. The aggregates are also maintained in the presence of a biologically relevant protein, bovine serum albumin (BSA), but become smaller (Figures S53−S60). Thus, these results suggest that complexes are introduced into cells mostly as aggregates, whose size decreases in the presence of biological proteins, a relevant finding that, to the best of our knowledge, has not been extensively studied for metallodrugs prior to this. Initially, the aggregates of compounds **1**, **2**, **5**, and **8** were observed around 150 nm, and those of **3**, **4**, and **6** were observed at 400−700 nm because of their lower solubility in this medium. This agrees with an increase of the absorption spectral baseline for these complexes, being more denoted for **3** and **6** with larger aggregates. The time intervals of 0, 1, 3, and 6 h were chosen because they are most pertinent with respect to the biological cultures. The observed variations of the size in the less soluble complexes may be ascribed to an increase of the self-assembled aggregates with time (in agreement with the larger broadening recorded in the NMR spectra), with those being maintained in the suspension smaller (in the case of **3**) or more homogeneous (sharper signals) in the case of **6**. A general increase in the aggregates' size is recorded for the more soluble samples, as expected for an aggregation process, which is more favored with time. Thus, the use of more soluble metallodrugs in a biological medium induces a slower kinetic self-assembly. Interestingly, smaller sizes were detected for those compounds with shorter Au···Au contacts (according to the X-ray crystal data), suggesting that

Table 3. Partition Coefficients for Compounds 1−8

compound	partition coefficient	log K_{ow}
1		
2		
3	2.1	0.3
4	4.5	0.7
5	1.2	0.1
6		
7		
8	6.9	0.8

https://doi.org/10.1021/acs.inorgchem.1c02359
Inorg. Chem. XXXX, XXX, XXX−XXX

aurophilicity favors the closer contacts between the molecules with respect to the more extended N−H···π assemblies.

Small-angle X-ray scattering (SAXS) experiments were also performed in the same solvent and concentration conditions to verify whether smaller aggregates may be present in the solutions at the biological temperature conditions. The use of this technique was relevant to identifying the presence of aggregated species at lower concentrations, such as those used for the biological experiments, which were more difficult to identify by other spectroscopic techniques. The low-resolution structures were reconstructed ab initio from the scattering patterns using the *DAMMIN* program. As can be observed in Table 4 and Figures S61−S69, small aggregates exist in all cases with sizes around 200−400 Å, which is additional evidence of the presence of aggregates in solutions of the studied metallodrugs.

Table 4. Sizes of the Small Aggregates of the Complexes Retrieved through SAXS Experiments under Conditions Analogous to Those Used for Biological Assays

	1	2	3	4	5	6	7	8
size (Å)	269	263	284	189	254	275	389	225

Previously we found a correlation between the complex internalization and cytotoxicity of mononuclear complexes, with higher intracellular concentrations of gold presenting lower IC_{50} values (higher cytotoxicity; Figure S70).[13] The same trend was observed for dinuclear complexes. However, dinuclear complexes with IC_{50} values similar to those of mononuclear complexes had higher intracellular percentages of gold.[13] This was the case for complexes **7** and **8** (both with IC_{50} = 0.3 μM) with internalizations of 41.7% and 34.4%, respectively, while complexes **4** (IC_{50} = 0.1 μM) and **5** (IC_{50} = 0.3 μM) presented 7.2% and 4.0%, respectively, of internalized gold.[13] Interestingly, when we compared this data with those from DLS, complexes **5**, **7**, and **8** with smaller aggregates (~200 nm) presented the same IC_{50} of 0.3 μM in ovarian cancer cells.[13] Larger aggregates (~ 300 nm) were recorded for **4**, with a lower IC_{50}. Hence, the formation of larger aggregates seems to be a positive point for obtaining better cytotoxicity values (lower IC_{50}). Because of the sensitivity of the inductively coupled plasma atomic emission spectrometry (ICP-AES) technique, analysis of complexes that presented gold internalization levels higher than 4% (complexes **4**, **5**, **7**, and **8**) was pursued. It must be said that, because of the high cytotoxicity of the complexes in ovarian cancer cells (low micromolar range),[13] biological studies performed at 48 h used the IC_{50} concentration of each complex, which is below c.a.c. Nevertheless, because the ICP-AES experiments were performed for shorter periods of incubation with the cells (to understand their internalization), the concentrations used in these cases were near the c.a.c., allowing better correlation with the above-described aggregation studies. Moreover, even in a more complex system (biological media with BSA), aggregation was still observed (see above). Indeed, the complexity of the biological media is even higher because it includes fetal bovine serum, which has different proteins besides BSA, and as described for other materials, a protein corona formation cannot be disregarded.[40]

It is expected that aggregates of complexes with more than 200 nm might require energy-dependent pathways, such as endocytosis for internalization.[41,53] Nevertheless, hydrophobic complexes might alter this internalization process because they are more soluble in the membrane lipids. Considering that the percentage of intracellular gold was evaluated in A2780 cells incubated with the complexes for 3 h at 4 °C, because the activity of cellular transporters is temperature-dependent, the energy-dependent mechanisms would be mostly inhibited at lower temperatures.[54,55] Figure 4 shows that, with the exception of complex **5**, only a slight decrease of the internalized gold was observed when the cells were incubated with the complexes at 4 °C relative to incubation at 37 °C, suggesting that complexes **4**, **7**, and **8** might enter A2780 cells via a passive mechanism. Regarding complex **5**, the percentage of gold inside cells decreased from 3.9% at 37 °C to 0.38% at 4 °C. Although it is tempting to assume that the lower internalization was due to the inhibition of active transport, because the uptake of complex **5** might be via an active transport mechanism, it is important to note that passive diffusion might also be affected by lower temperature. A comparison with the absorption, emission, and SAXS data performed at 37 °C also supports the postulation that in all cases the aggregates are the internalized species at this temperature.

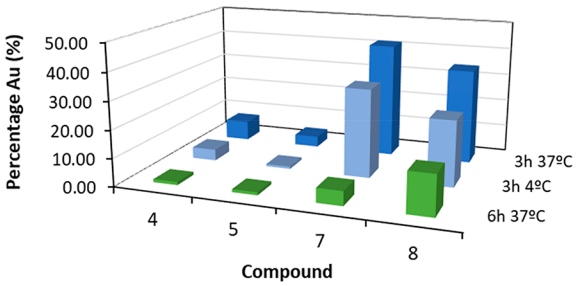

Figure 4. Internalization of complexes **4**, **5**, **7**, and **8** in ovarian cancer cells A2780 after 3 h at 37 °C (dark blue) and 4 °C (light blue) and after 6 h at 37 °C (green). Bars represent the percentage of gold in cells relative to the total amount of gold found in the media and cells for each sample.

In line with the results previously observed for complex **3**,[13] a decrease of the internalization is observed after 6 h in all complexes, with complex **7** showing the highest deviation, from 41.7% internalized gold after 3 h to 5.2% internalized gold after 6 h (Figure 4). This decrease of the internalization of complexes might be correlated, as in the case of **8**, with the increased size of aggregates over time, as observed by DLS (Figure S52), or possibly precipitation over time (due to low water solubility; Table 3).

A dark-field microscopy analysis was performed to understand whether complexes with higher log K_{ow} values were internalized by cells in the aggregated form. The A2780 cells were exposed for 3 h with the IC_{50} values of complexes **4** and **8** or with 0.1% (v/v) DMSO as the control sample. The results showed that cells incubated with complex **4** displayed brighter spots at the membrane, consistent with a denser material and, hence, with the presence of complex **4** aggregates (Figure 5). These results suggest that aggregates of complex **4** interact with the cell membranes and might be internalized.

To further understand the possible uptake of complexes by passive mechanisms, particularly for complexes **4**, **7**, and **8** (**5** was also included for comparison), their partition coefficients were analyzed (Table 3). Interestingly, compounds **4** and **8** show higher partition coefficients, which agrees with their

https://doi.org/10.1021/acs.inorgchem.1c02359
Inorg. Chem. XXXX, XXX, XXX−XXX

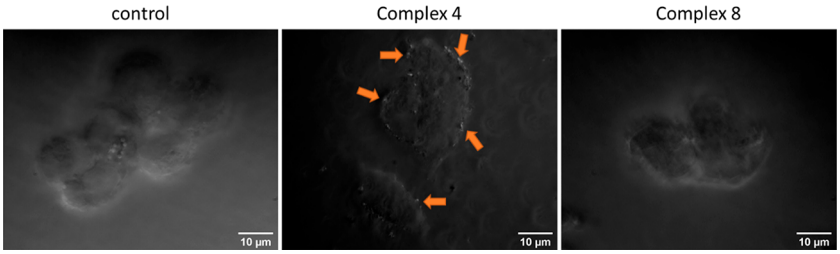

Figure 5. Analysis of the internalization in the aggregated form of complexes **4** and **8**. The ovarian cancer cell line A2780 was incubated for 3 h with the IC_{50} values of each complex (0.1 μM for complex **4** and 0.3 μM for complex **8**) or 0.1% (v/v) DMSO for control purposes and then fixed with formaldehyde 4% (w/v). Images were acquired in an Eclipse Ti−U inverted microscope using a dark-field condenser. Orange arrows point to bright spots consistent with the presence of complex **4** as aggregates.

higher affinity for membrane lipids and possible diffusion through them compared to complex **5**, as stated above. Altogether, the results suggest that, although the internalization of complex aggregates might not be excluded, as observed in Figure 5, the higher cytotoxicity of **4** might be correlated with its lower size of aggregates recorded by SAXS (Table 4) and its hydrophobicity that can more easily cross cell membranes via passive transport (Table 3).

Previously we demonstrated that complex **3** induced intrinsic apoptosis in A2780 cells, possibly because of increased reactive oxygen species production.[13] To further enlighten the effect of the complexes on A2780 cells, the intracellular distribution within cellular organelles was accessed through cellular fractionation using a detergent-based cell fractionation kit (Cell Signaling Technologies). With this methodology, it is possible to separate the cell content into three fractions: the "cytosolic fraction", the "mitochondrial fraction" composed of membranes and organelles, and the "nuclear fraction" composed of nuclei and cytoskeletons. The distribution of the complexes throughout the cell fractions was evaluated by ICP-AES. Interestingly, the results suggest that while the original mononuclear complexes are mainly found in the cytosolic fraction, the original dinuclear complexes (**7** and **8**) are mainly in the later fraction comprised of nuclei and cytoskeletons (Figure 6).

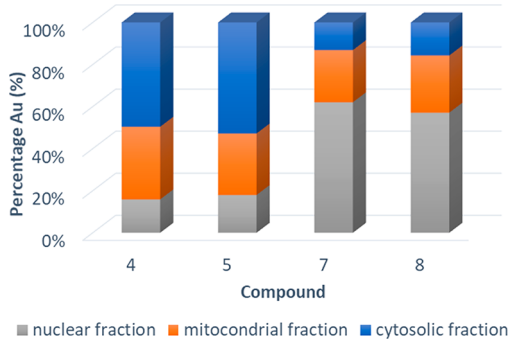

Figure 6. Distribution of complexes **4**, **5**, **7**, and **8** in the ovarian carcinoma cell line A2780. Cells were exposed to 10 × IC_{50} of each complex for 3 h at 37 °C. Cells were then fractionated using a cell fractionation kit (Cell Signaling Technologies) into the cytosolic fraction, mitochondrial fraction (composed of membranes and organelles), and nuclear fraction (composed of nuclei and cytoskeletons). The concentration of gold in each fraction was measured by ICP-AES, and the represented percentage of gold in each bar is the gold in each fraction relative to the sum of gold in all fractions.

Because of the high percentage of complexes in the nuclear/cytoskeleton fraction, it was examined whether the complexes interact with actin. With this purpose, A2780 cells were exposed for 0−6 h to the IC_{50} concentration of the mononuclear complex **4** (0.1 μM) or to the IC_{50} concentration of the dinuclear complex **8** (0.3 μM). Afterward, cells were fixed with formaldehyde, and actin stained with phalloidin (Figures 7 and S71).

The results show that both complexes presented some interaction with actin, causing the formation of actin agglomerations, which is consistent with actin disruptions.[56,57] However, while actin aggregates are present in the cells incubated with complex **4** for 30 min or 1 h, major actin modifications are mainly observed after a 3 h of incubation with complex **8** (Figure 7). A closer look at A2780 cells incubated with both complexes for 3 h revealed that that the actin filaments in cells incubated with complex **8** were more disorganized than those in cells incubated with DMSO (control conditions) or with complex **4**. These results might suggest that complex **8** destabilizes the actin cytoskeleton of the cells in a major degree probably because of cooperative effects between the two gold(I) moieties.[58] The interaction of gold compounds with actin or actin-related proteins in A2780 cells was previously described in a proteomic analysis by Messori, Modesti, and co-workers,[23] where they observed a decreased expression of two actin isoforms when cells were incubated with auranofin and Auoxo6. The cytoskeleton modification and/or reorganization was frequently correlated with apoptosis.[23,59]

Nevertheless, aggregation does not seem to affect this process because both complexes **4** and **8** present similar aggregation sizes after 3−6 h. Thus, aggregation seems to be involved in a possible passive mechanism to enter the cells, but the final biological action (once the compounds are already within the cells) is expected to be more susceptible to a cooperative effect related to the nuclearity of the metallodrugs.

CONCLUSIONS

Intermolecular interactions in terms of N−H···π or aurophilic contacts play a key role in the aggregation process of a series of gold(I) metallodrugs, as observed in the X-ray crystal packing, and these aggregates are maintained in solution even at very low concentrations. SAXS experiments were very useful for detecting the presence of small aggregates (200−400 Å) that can give rise to larger structures (>1000 Å), as detected by DLS.

Correlation between the previously studied biological activity and aggregation motifs determined that the samples are already incorporated within the cells as aggregates that pass

https://doi.org/10.1021/acs.inorgchem.1c02359
Inorg. Chem. XXXX, XXX, XXX−XXX

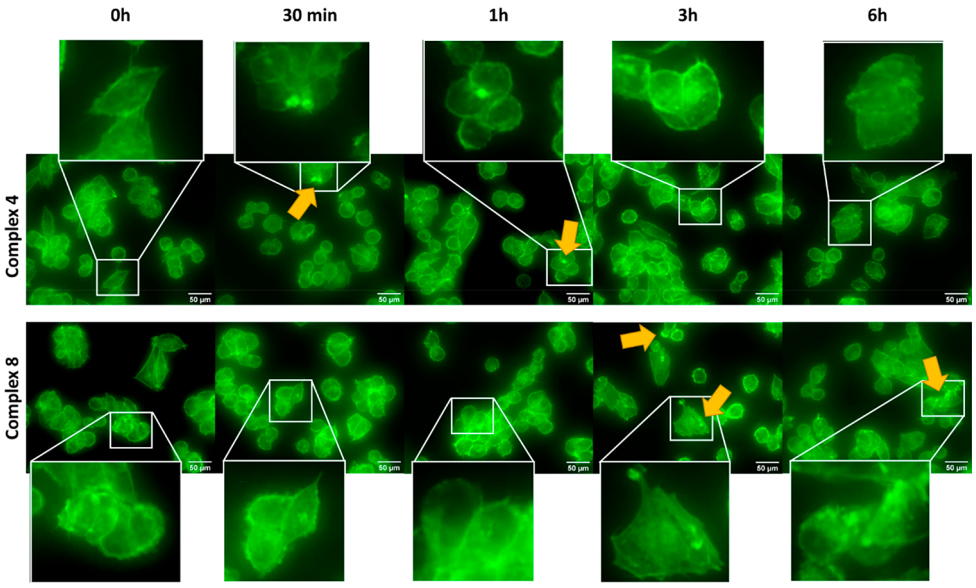

Figure 7. Interaction of complexes **4** and **8** with actin. The ovarian cancer cell line A2780 was incubated for 0 h, 30 min, 1 h, 3 h, and 6 h with the IC_{50} value of each complex (0.1 μM for complex **4** and 0.3 μM for complex **8**) and then fixed with formaldehyde 4% (w/v). Cells were stained with AlexaFluor 488 phalloidin (Invitrogen), and images were acquired on an Eclipse Ti−U inverted microscope with a green filter cube (excitation filter range at 465−495 nm and emission filter range at 515−555 nm). Orange arrows point to actin agglomerations in cells.

through the cellular membranes, possibly through a passive diffusion mechanism. Nevertheless, once inside the cells, their biological activity and subcellular localization seem to be more correlated with the original nuclearity of the complexes. These preliminary studies indicate that a wider array of complexes should be analyzed in order to obtain additional evidence that the nuclearity may favor the targeting of complexes to specific biological subcellular compartments.

To the best of our knowledge, a study of the mechanism of entering the cells in these types of complexes has no precedent in the literature and is of great relevance to better understand their behavior and toward increased efficacy in the future drug design of metallodrugs.

EXPERIMENTAL SECTION

General Procedures. All manipulations were performed under prepurified N_2 using standard Schlenk techniques. All solvents were distilled from the appropriate drying agents. Literature methods were used to prepare 4-ethynylaniline gold(I) complexes containing monophosphane [1,3,5-triaza-7-phosphaadamantane (pta; **1**), 3,7-diacetyl-1,3,7-triaza-5-phosphabicyclo[3.3.1]nonane (**2**), and PR_3, with R = naphthyl (**3**), phenyl (**4**), and ethyl (**5**)] and diphosphane [bis(diphenylphosphino)acetylene (dppa; **6**), 1,2-bis(diphenylphosphino)ethane (dppe; **7**), and 1,3-bis(diphenylphosphino)propane (dppp; **8**)].[13]

Physical Measurements. IR spectra were recorded on a Nicolet FT-IR 520 spectrophotometer. ^{1}H NMR [δ(TMS) = 0.0 ppm] and ^{31}P{^{1}H} NMR [δ(85% H_3PO_4) = 0.0 ppm] spectra were obtained on Varian Mercury 400 and Bruker 400 spectrometers (Universitat de Barcelona). Electrospray ionization mass spectrometry (positive-ion mode) spectra were recorded on a Fisons VG Quatro spectrometer (Universitat de Barcelona). Absorption spectra were recorded on a Varian Cary 100 Bio UV- spectrophotometer and emission spectra on a Horiba-Jobin-Ybon SPEX Nanolog spectrofluorimeter (Universitat de Barcelona). DLS spectra were obtained on a Zetasizer Nano S of Malvern (Parc Científic de Barcelona). The samples were measured in quartz cuvettes. SAXS was performed on the NCD-SWEET beamline at the ALBA Synchrotron at 12.4 keV, and the sample/detector distance was 6.2 m to cover the range of momentum transfer of 0.028 $nm^{-1} < q < 2.56\ nm^{-1}$. The data were collected on a Pilatus3S 1 M detector with a pixel size of 172.0 × 172.0 μm^2. The exposure time was 30 s. The q-axis calibration was obtained by measuring silver behenate.[60] The program *pyFAI* was used to integrate the 2D SAXS data into 1D data.[61] The data were then subtracted by the background using *PRIMUS* software.[62] The maximum particle dimension D_{max} and the pair distance distribution $P(r)$ were determined with *GNOM*.[62] The low-resolution structure of the aggregates was reconstructed ab initio from the initial portions of the scattering patterns using the *DAMMIN* program.[63]

X-ray Crystal Structure Determination. The crystal data and experimental details for the data collection of **1a** (CCDC 2070637), **1b** (CCDC 2070638), **4** (CCDC 2070639), and **5** (CCDC 2070640) are given in Table S1. The single-crystal data for **1a**, **1b**, and **4** were collected using a Bruker-Nonius Kappa CCD diffractometer with an APEX-II detector with graphite-monochromatized Mo Kα (λ = 0.71073 Å) radiation. Data collection and reduction were performed using the programs *COLLECT*[64] and *HKL DENZO AND SCALEPACK*,[65] respectively, and the intensities were corrected for absorption using *SADABS*.[66] Single-crystal X-ray data for **5** were measured using a Rigaku SuperNova dual-source Oxford diffractometer equipped with an Atlas detector using mirror-monochromated Cu Kα (λ = 1.54184 Å) radiation. Data collection and reduction were performed using the program *CrysAlisPro*.[67] The structures were solved with intrinsic phasing (*SHELXT*).[68] Non-hydrogen atoms were assigned anisotropic displacement parameters unless stated otherwise. Hydrogen atoms were placed in idealized positions and included as riding. The isotropic displacement parameters for all hydrogen atoms were constrained to multiples of the equivalent displacement parameters of their parent atoms with $U_{iso}(H) = 1.2U_{eq}$(parent atom).

Aggregation Studies. The c.a.c. was obtained by recording the absorption, excitation, and emission spectra at different concentrations (5×10^{-5}−10^{-6} M) in a mixture of DMSO and water (50:50 in the case of **1**−**5** and **8** or 60:40 in the case of **6** and **7**).

NMR studies at different concentrations (5.5×10^{-3}−2.4×10^{-4}) were carried out by dissolving the corresponding quantity of compound in a DMSO-d_6/D_2O mixture (50:50 in the case of **1**−**5** and **8** or 60:40 in the case of **6** and **7**).

The samples for SAXS were prepared 1 week before in order to favor the aggregation processes at different concentrations (10^{-4}−5×10^{-6} M) in water for **1** and **2** and in water/tetrahydrofuran mixtures (50:50) for **3**−**8**.

https://doi.org/10.1021/acs.inorgchem.1c02359
Inorg. Chem. XXXX, XXX, XXX−XXX

Time-dependent studies of 10^{-5} M water solutions containing 0.1% DMSO were followed by absorption spectroscopy and DLS at different times (0, 1, 3, and 6 h) at 37 °C.

Partition Coefficient. The partition coefficient was calculated following literature methods.[69]

Biological Assays. *Cell Culture and Cell Culture Maintenance.* Human ovarian carcinoma, A2780, purchased from ATCC (Manassas, VA) was grown and maintained in an RPMI 1640 medium (Gibco, ThermoFisher Scientific, Waltham, MA), supplemented with 10% (v/v) fetal bovine serum (Gibco, ThermoFisher Scientific), 1% (v/v) nonessential amino acids (MEM; Gibco, ThermoFisher Scientific), and a mixture of 100 U/mL penicillin and 100 μg/mL streptomycin (Gibco, ThermoFisher Scientific) at 37 °C and 5% (v/v) CO_2 in an humidified atmosphere.[70]

*Cellular Uptake of Complexes **4**, **5**, **7**, and **8** by A2780 Cells.* To evaluate the internalization of the complexes, 2×10^6 A2780 cells were seeded in a 25 cm^2 T-flask and allowed to adhere for 24 h. Afterward, the media were replaced by fresh media supplemented with 10 times the respective IC_{50} value of each complex and incubated for 3 h at 37 and 4 °C or for 6 h at 37 °C. The supernatant was transferred to a clean tube, and the cells were washed with PBS that was added to the supernatant-containing tube. The cells were then detached with TrypLE Express (ThermoFisher Scientific) and pelleted with 500*g* centrifugation for 5 min. The supernatant was transferred to the supernatant-containing tube, and both the cells and supernatant samples were incubated with aqua regia overnight. The amount of gold in each sample was quantified with ICP-AES. The percentage of intracellular gold was calculated by dividing the gold concentration in the cells by the sum of the gold concentrations in the respective supernatants and cell pellets.[13]

*Distribution of Complexes **4**, **5**, **7**, and **8** in Cellular Fractions.* A2780 cells were seeded in 25 cm^2 T-flasks in a density of 6×10^5 cells/mL. After 24 h, the cells were exposed to fresh media supplemented with $10 \times IC_{50}$ of each complex and incubated for 3 h at 37 °C and 5% (v/v) CO_2 in a humidified atmosphere. Afterward, the cells were collected with a cell scratcher in PBS, pelleted with 500*g* centrifugation for 5 min, and fractionated with a Cell Fractionation Kit (Cell Signaling Technologies, Danvers, MA) according to the manufacturer's instructions. With this protocol, three fractions were obtained: the cytoplasmic fraction, mitochondrial fraction, composed of membranes and organelles, and nuclear fraction. After incubation of each obtained fraction with aqua regia, the amount of gold was quantified with ICP-AES. The percentage of gold in each fraction was calculated by dividing the gold concentration in the specific fraction with the sum of the gold concentrations in the respective cytoplasmic, mitochondrial, and nuclear fractions.

*Interaction of Complexes **4** and **8** with Actin.* A2780 cells were seeded in a 24-well plate in a cell density of 37500 cells/well. After 24 h, the media were replaced by the IC_{50} value of complex **4** (0.1 μM), the IC_{50} value of complex **8** (0.3 μM), or 0.1% (v/v) DMSO, the vehicle solvent of the complexes. After 0 h, 30 min, 1 h, 3 h, or 6 h of incubation, the cells were fixed with 4% (w/v) formaldehyde (Sigma-Aldrich, Merck, Kenilworth, NJ) for 15 min and washed three times with PBS. The cell membrane was then disrupted by a 5 min incubation with 0.1% (v/v) Triton (Sigma-Aldrich, Merck) and washed three times with PBS, and the cells were incubated for 30 min with 1% (w/v) bovine serum albumin (BSA; NZYtech, Lisbon, Portugal) and 20 min with AlexaFluor 488 phalloidin (Invitrogen, ThermoFisher Scientific), as previously described.[71] After washing three times with PBS, the cells were visualized with an Eclipse Ti–U inverted microscope with a green filter cube (an excitation filter range at 465–495 nm and an emission filter range at 515–555 nm), and images were acquired with the respective microscope software. Three different images with around 20 cells were acquired per sample with a 40× objective, or five different images with around five cells were acquired with a 100× objective.

Dark-Field Analysis. A2780 cells were seeded in a 24-well plate in a cell density of 37500 cells/well. After 24 h, the media were replaced by the IC_{50} value of complex **4** (0.1 μM), the IC_{50} value of complex **8** (0.3 μM), or 0.1% (v/v) DMSO, the vehicle solvent of the complexes. After 3 h of incubation, the cells were fixed with 4% (w/v) formaldehyde (Sigma-Aldrich, Merck) for 15 min and washed three times with PBS. The cells were visualized with an Eclipse Ti–U inverted microscope using a dark-field condenser and a 100× objective. Five different images with around five cells were acquired per sample.

■ ASSOCIATED CONTENT

Supporting Information

The Supporting Information is available free of charge at https://pubs.acs.org/doi/10.1021/acs.inorgchem.1c02359.

X-ray packing of the molecules, absorption and emission spectra of the compounds at different concentrations, emission spectra of the compounds at different temperatures, ^{1}H and ^{31}P NMR spectra of the compounds at different concentrations in a mixture of D_2O/DMSO-d_6, absorption spectra of the compounds at different times, DLS spectra of the compounds at different times, SAXS data of the compounds at diluted conditions, plot representing the percentage of gold internalized versus IC_{50} values against the A2780 cell line, interaction of complexes **4** and **8** with actin, crystal data and structures for **1a**, **1b**, **4**, and **5**, and internalization data of complexes **4**, **5**, **7**, and **8** in ovarian cancer cells A2780 after 3 h at 37 and 4 °C and after 6 h at 37 °C (PDF)

Accession Codes

CCDC 2070637–2070640 contain the supplementary crystallographic data for this paper. These data can be obtained free of charge via www.ccdc.cam.ac.uk/data_request/cif, or by emailing data_request@ccdc.cam.ac.uk, or by contacting The Cambridge Crystallographic Data Centre, 12 Union Road, Cambridge CB2 1EZ, UK; fax: +44 1223 336033.

■ AUTHOR INFORMATION

Corresponding Authors

Alexandra R. Fernandes − *UCIBIO—Applied Molecular Biosciences Unit, Department of Life Sciences and Associate Laboratory i4HB, Institute for Health and Bioeconomy, NOVA School of Science and Technology, NOVA University Lisbon, 2819-516 Caparica, Portugal;* orcid.org/0000-0003-2054-4438; Email: ma.fernandes@fct.unl.pt

Laura Rodríguez − *Departament de Química Inorgànica i Orgànica, Secció de Química Inorgànica, Universitat de Barcelona, E-08028 Barcelona, Spain; Institut de Nanociència i Nanotecnologia (IN^{2}UB), Universitat de Barcelona, 08028 Barcelona, Spain;* orcid.org/0000-0003-1289-1587; Email: laura.rodriguez@qi.ub.es

Authors

Andrea Pinto − *Departament de Química Inorgànica i Orgànica, Secció de Química Inorgànica, Universitat de Barcelona, E-08028 Barcelona, Spain; Institut de Nanociència i Nanotecnologia (IN^{2}UB), Universitat de Barcelona, 08028 Barcelona, Spain*

Catarina Roma-Rodrigues − *UCIBIO—Applied Molecular Biosciences Unit, Department of Life Sciences and Associate Laboratory i4HB, Institute for Health and Bioeconomy, NOVA School of Science and Technology, NOVA University Lisbon, 2819-516 Caparica, Portugal*

Jas S. Ward − *Department of Chemistry, University of Jyvaskyla, 40014 Jväskylä, Finland;* orcid.org/0000-0001-9089-9643

https://doi.org/10.1021/acs.inorgchem.1c02359
Inorg. Chem. XXXX, XXX, XXX−XXX

Rakesh Puttreddy − *Faculty of Engineering and Natural Sciences, Tampere University, FI-33101 Tampere, Finland;* orcid.org/0000-0002-2221-526X

Kari Rissanen − *Department of Chemistry, University of Jyvaskyla, 40014 Jväskylä, Finland;* orcid.org/0000-0002-7282-8419

Pedro V. Baptista − *UCIBIO—Applied Molecular Biosciences Unit, Department of Life Sciences and Associate Laboratory i4HB, Institute for Health and Bioeconomy, NOVA School of Science and Technology, NOVA University Lisbon, 2819-516 Caparica, Portugal;* orcid.org/0000-0001-5255-7095

João Carlos Lima − *LAQV-REQUIMTE, Departamento de Química, CQFB, Universidade Nova de Lisboa, 2825-152 Monte de Caparica, Portugal;* orcid.org/0000-0003-0528-1967

Complete contact information is available at: https://pubs.acs.org/10.1021/acs.inorgchem.1c02359

Author Contributions

†These authors made equal contributions.

Notes

The authors declare no competing financial interest.

■ ACKNOWLEDGMENTS

The authors are grateful to the Spanish Ministerio de Ciencia, Innovación y Universidades (Project PID2019-104121GB-I00). This work was supported by the Associate Laboratory for Green Chemistry, LAQV, which is financed by national funds from FCT/MCTES (Grants UIDB/50006/2020 and UIDP/50006/2020). This work was also financed by national funds from Fundação para a Ciência e a Tecnologia, I.P., in the scope of Projects UIDP/04378/2020 and UIDB/04378/2020 of the Research Unit on Applied Molecular Biosciences, UCIBIO, and Project LA/P/0140/2020 of the Associate Laboratory Institute for Health and Bioeconomy, i4HB. SAXS experiments were performed at the NCD-BL11 beamline of the ALBA Synchrotron Light Facility in collaboration with the ALBA staff. The authors also acknowledge COST Actions CA1740—Nano4clinics and CA18202—NECTAR. The Finnish Cultural Foundation (Grant 00201148 to J.S.W.) is also acknowledged for their support.

■ REFERENCES

(1) Rubbiani, R.; Wahrig, B.; Ott, I. Historical and Biochemical Aspects of a Seventeenth Century Gold-Based Aurum Vitae Recipe. *JBIC, J. Biol. Inorg. Chem.* **2014**, *19* (6), 961−965.

(2) [illegible]s Lima, J.; Rodriguez, L. Phosphine-Gold(I) Compounds as Anticancer Agents: General Description and Mechanisms of Action. *Anti-Cancer Agents Med. Chem.* **2011**, *11* (10), 921−928.

(3) (a) Kupiec, M.; Ziółkowski, R.; Massai, L.; Messori, L.; Pawlak, K. The Electrochemical Profiles of Auranofin and Aubipyc, Two Representative Medicinal Gold Compounds: A Comparative Study. *J. Inorg. Biochem.* **2019**, *198*, 110714. (b) Jakob, C. H. G.; Muñoz, A. W.; Schlagintweit, J. F.; Weiß, V.; Reich, R. M.; Sieber, S. A.; Correia, J. D. G.; Kühn, F. E. Anticancer and antibacterial properties of trinuclear Cu(I), Ag(I) and Au(I) macrocyclic NHC/urea complexes. *J. Organomet. Chem.* **2021**, *932*, 121643.

(4) (a) Palermo, G.; Spinello, A.; Saha, A.; Magistrato, A. Frontiers of Metal-Coordinating Drug Design. *Expert Opin. Drug Discovery* **2021**, *16* (5), 497−511. (b) Zhang, J.-J.; Abu el Maaty, M. A.; Hoffmeister, H.; Schmidt, C.; Muenzner, J. K.; Schobert, R.; Wölfl, S.; Ott, I. A Multitarget Gold(I) Complex Induces Cytotoxicity Related to Aneuploidy in HCT-116 Colorectal Carcinoma Cells. *Angew. Chem., Int. Ed.* **2020**, *59*, 16795−16800.

(5) (a) Tolbatov, I.; Coletti, C.; Marrone, A.; Re, N. Insight into the Substitution Mechanism of Antitumor Au(I) N-Heterocyclic Carbene Complexes by Cysteine and Selenocysteine. *Inorg. Chem.* **2020**, *59* (5), 3312−3320. (b) Bian, M.; Sun, Y.; Liu, Y.; Xu, Z.; Fan, R.; Liu, Z.; Liu, W. A Gold(I) Complex Containing an Oleanolic Acid Derivative as a Potential Anti-Ovarian-Cancer Agent by Inhibiting TrxR and Activating ROS-Mediated ERS. *Chem. - Eur. J.* **2020**, *26*, 7092−7108.

(6) (a) Mármol, I.; Montanel-Perez, S.; Royo, J. C.; Gimeno, M. C.; Villacampa, M. D.; Rodríguez-Yoldi, M. J.; Cerrada, E. Gold(I) and Silver(I) Complexes with 2-Anilinopyridine-Based Heterocycles as Multitarget Drugs against Colon Cancer. *Inorg. Chem.* **2020**, *59* (23), 17732−17745. (b) Morgen, M.; Fabrowski, P.; Amtmann, E.; Gunkel, N.; Miller, A. K. Inclusion Complexes of Gold(I)-Dithiocarbamates with β-Cyclodextrin: A Journey from Drug Repurposing towards Drug Discovery. *Chem. - Eur. J.* **2021**, *27*, 12156−12165.

(7) (a) Silva, M. J. S. A.; Gois, P. M. P.; Gasser, G. Unveiling the Potential of Transition Metal Complexes for Medicine: Translational in Situ Activation of Metal-Based Drugs from Bench to in Vivo Applications. *ChemBioChem* **2021**, *22* (10), 1740−1742. (b) Bayrakdar, T.A. C. A.; Scattolin, T.; Ma, X.; Nolan, S. P. Dinuclear gold(I) complexes: from bonding to applications. *Chem. Soc. Rev.* **2020**, *49*, 7044−7100.

(8) Redrado, M.; Fernández-Moreira, V.; Gimeno, M. C. Theranostics Through the Synergistic Cooperation of Heterometallic Complexes. *ChemMedChem* **2021**, *16* (6), 932−941.

(9) Johnson, A.; Marzo, I.; Gimeno, M. C. Heterobimetallic Propargyl Gold Complexes with π-Bound Copper or Silver with Enhanced Anticancer Activity. *Dalton Trans.* **2020**, *49* (33), 11736−11742.

(10) Odachowski, M.; Marschner, C.; Blom, B. A Review on 1,1-Bis(Diphenylphosphino)Methane Bridged Homo- and Heterobimetallic Complexes for Anticancer Applications: Synthesis, Structure, and Cytotoxicity. *Eur. J. Med. Chem.* **2020**, *204*, 112613.

(11) Marzo, T.; Messori, L. A Role for Metal-Based Drugs in Fighting COVID-19 Infection? The Case of Auranofin. *ACS Med. Chem. Lett.* **2020**, *11* (6), 1067−1068.

(12) Gil-Moles, M.; Basu, U.; Büssing, R.; Hoffmeister, H.; Türck, S.; Varchmin, A.; Ott, I. Gold Metallodrugs to Target Coronavirus Proteins: Inhibitory Effects on the Spike-ACE2 Interaction and on PLpro Protease Activity by Auranofin and Gold Organometallics. *Chem. - Eur. J.* **2020**, *26* (66), 15140−15144.

(13) Svahn, N.; Moro, A. J.; Roma-Rodrigues, C.; Puttreddy, R.; Rissanen, K.; Baptista, P. V.; Fernandes, A. R.; Lima, J. C.; Rodríguez, L. The Important Role of the Nuclearity, Rigidity, and Solubility of Phosphane Ligands in the Biological Activity of Gold(I) Complexes. *Chem. - Eur. J.* **2018**, *24* (55), 14654−14667.

(14) Meyer, A.; Bagowski, C. P.; Kokoschka, M.; Stefanopoulou, M.; Alborzinia, H.; Can, S.; Vlecken, D. H.; Sheldrick, W. S.; Wölfl, S.; Ott, I. On the Biological Properties of Alkynyl Phosphine Gold(I) Complexes. *Angew. Chem., Int. Ed.* **2012**, *51* (35), 8895−8899.

(15) Mármol, I.; Castellnou, P.; Alvarez, R.; Gimeno, M. C.; Rodríguez-Yoldi, M. J.; Cerrada, E. Alkynyl Gold(I) Complexes Derived from 3-Hydroxyflavones as Multi-Targeted Drugs against Colon Cancer. *Eur. J. Med. Chem.* **2019**, *183*, 111661.

(16) Andermark, V.; Göke, K.; Kokoschka, M.; Abu el Maaty, M. A.; Lum, C. T.; Zou, T.; Sun, R. W.-Y.; Aguiló, E.; Oehninger, L.; Rodríguez, L.; Bunjes, H.; Wölfl, S.; Che, C.-M.; Ott, I. Alkynyl Gold(I) Phosphane Complexes: Evaluation of Structure−Activity-Relationships for the Phosphane Ligands, Effects on Key Signaling Proteins and Preliminary in-Vivo Studies with a Nanoformulated Complex. *J. Inorg. Biochem.* **2016**, *160*, 140−148.

(17) Chui, C.-H.; Wong, R. S.-M.; Gambari, R.; Cheng, G. Y.-M.; Yuen, M. C.-W.; Chan, K.-W.; Tong, S.-W.; Lau, F.-Y.; Lai, P. B.-S.; Lam, K.-H.; Ho, C.-L.; Kan, C.-W.; Leung, K. S.-Y.; Wong, W.-Y. Antitumor Activity of Diethynylfluorene Derivatives of Gold(I). *Bioorg. Med. Chem.* **2009**, *17* (23), 7872−7877.

(18) Meyer, A.; Gutiérrez, A.; Ott, I.; Rodríguez, L. Phosphine-Bridged Dinuclear Gold(I) Alkynyl Complexes: Thioredoxin

Reductase Inhibition and Cytotoxicity. *Inorg. Chim. Acta* **2013**, *398*, 72−76.
(19) Gavara, R.; Aguiló, E.; Schur, J.; Llorca, J.; Ott, I.; Rodríguez, L. Study of the Effect of the Chromophore and Nuclearity on the Aggregation and Potential Biological Activity of Gold(I) Alkynyl Complexes. *Inorg. Chim. Acta* **2016**, *446*, 189−197.
(20) Dalmases, M.; Pinto, A.; Lippmann, P.; Ott, I.; Rodríguez, L.; Figuerola, A. Preparation and Antitumoral Activity of Au-Based Inorganic-Organometallic Nanocomposites. *Front. Chem.* **2019**, *7* (FEB), 1−10.
(21) Casini, A. Exploring the Mechanisms of Metalbased Pharmacological Agents via an Integrated Approach. *J. Inorg. Biochem.* **2012**, *109*, 97−106.
(22) Wang, Y.; Li, H.; Sun, H. Metalloproteomics for Unveiling the Mechanism of Action of Metallodrugs. *Inorg. Chem.* **2019**, *58* (20), 13673−13685.
(23) Guidi, F.; Landini, I.; Puglia, M.; Magherini, F.; Gabbiani, C.; Cinellu, M. A.; Nobili, S.; Fiaschi, T.; Bini, L.; Mini, E.; Messori, L.; Modesti, A. Proteomic Analysis of Ovarian Cancer Cell Responses to Cytotoxic Gold Compounds. *Metallomics* **2012**, *4* (3), 307.
(24) Rackham, O.; Nichols, S. J.; Leedman, P. J.; Berners-Price, S. J.; Filipovska, A. A Gold(I) Phosphine Complex Selectively Induces Apoptosis in Breast Cancer Cells: Implications for Anticancer Therapeutics Targeted to Mitochondria. *Biochem. Pharmacol.* **2007**, *74* (7), 992−1002.
(25) Meyer, A.; Grotefend, S.; Gross, A.; Wätzig, H.; Ott, I. Total Reflection X-Ray Fluorescence Spectrometry as a Tool for the Quantification of Gold and Platinum Metallodrugs: Determination of Recovery Rates and Precision in the Ppb Concentration Range. *J. Pharm. Biomed. Anal.* **2012**, *70*, 713−717.
(26) Loreto, D.; Ferraro, G.; Merlino, A. Protein-Metallodrugs Interactions: Effects on the Overall Protein Structure and Characterization of Au, Ru and Pt Binding Sites. *Int. J. Biol. Macromol.* **2020**, *163*, 970−976.
(27) de Almeida, A.; Mósca, A. F.; Wragg, D.; Wenzel, M.; Kavanagh, P.; Barone, G.; Leoni, S.; Soveral, G.; Casini, A. The Mechanism of Aquaporin Inhibition by Gold Compounds Elucidated by Biophysical and Computational Methods. *Chem. Commun.* **2017**, *53* (27), 3830−3833.
(28) Jacques, A.; Lebrun, C.; Casini, A.; Kieffer, I.; Proux, O.; Latour, J.-M.; Sénèque, O. Reactivity of Cys 4 Zinc Finger Domains with Gold(III) Complexes: Insights into the Formation of "Gold Fingers. *Inorg. Chem.* **2015**, *54* (8), 4104−4113.
(29) Meier-Menches, S. M.; Aikman, B.; Döllerer, D.; Klooster, W. T.; Coles, S. J.; Santi, N.; Luk, L.; Casini, A.; Bonsignore, R. Comparative Biological Evaluation and G-Quadruplex Interaction Studies of Two New Families of Organometallic Gold(I) Complexes Featuring N-Heterocyclic Carbene and Alkynyl Ligands. *J. Inorg. Biochem.* **2020**, *202*, 110844.
(30) Wragg, D.; de Almeida, A.; Bonsignore, R.; Kühn, F. E.; Leoni, S.; Casini, A. On the Mechanism of Gold/NHC Compounds Binding to DNA G-Quadruplexes: Combined Metadynamics and Biophysical Methods. *Angew. Chem., Int. Ed.* **2018**, *57* (44), 14524−14528.
(31) Pujadas, M.; Rodríguez, L. Luminescent Phosphine Gold(I) Alkynyl Complexes. Highlights from 2010 to 2018. *Coord. Chem. Rev.* **2020**, *408*, 213179.
(32) Raubenheimer, H. G.; Schmidbaur, H. Gold Chemistry Guided by the Isolobality Concept. *Organometallics* **2012**, *31* (7), 2507−2522.
(33) Aguiló, E.; Moro, A. J.; Gavara, R.; Alfonso, I.; Pérez, Y.; Zaccaria, F.; Guerra, C. F.; Malfois, M.; Baucells, C.; Ferrer, M.; Lima, J. C.; Rodríguez, L. Reversible Self-Assembly of Water-Soluble Gold(I) Complexes. *Inorg. Chem.* **2018**, *57* (3), 1017−1028.
(34) Gavara, R.; Aguiló, E.; Fonseca Guerra, C.; Rodríguez, L.; Lima, J. C. Thermodynamic Aspects of Aurophilic Hydrogelators. *Inorg. Chem.* **2015**, *54* (11), 5195−5203.
(35) Moro, A. J.; Rome, B.; Aguiló, E.; Arcau, J.; Puttreddy, R.; Rissanen, K.; Lima, J. C.; Rodríguez, L. A Coumarin Based Gold(I)-Alkynyl Complex: A New Class of Supramolecular Hydrogelators. *Org. Biomol. Chem.* **2015**, *13* (7), 2026−2033.
(36) Lima, J. C.; Rodríguez, L. Supramolecular Gold Metallogelators: The Key Role of Metallophilic Interactions. *Inorganics* **2015**, *3* (1), 1−18.
(37) Pinto, A.; Svahn, N.; Lima, J. C.; Rodríguez, L. Aggregation Induced Emission of Gold(I) Complexes in Water or Water Mixtures. *Dalton Trans.* **2017**, *46* (34), 11125−11139.
(38) Gavara, R.; Pinto, A.; Donamaría, R.; Olmos, M. E.; López de Luzuriaga, J. M.; Rodríguez, L. Polarized Supramolecular Aggregates Based on Luminescent Perhalogenated Gold Derivatives. *Inorg. Chem.* **2017**, *56* (19), 11946−11955.
(39) Pinto, A.; Hernández, G.; Gavara, R.; Aguiló, E.; Moro, A. J.; Aullón, G.; Malfois, M.; Lima, J. C.; Rodríguez, L. Supramolecular Tripodal Au(I) Assemblies in Water. Interactions with a Pyrene Fluorescent Probe. *New J. Chem.* **2019**, *43* (21), 8279−8289.
(40) Caracciolo, G.; Callipo, L.; De Sanctis, S. C.; Cavaliere, C.; Pozzi, D.; Laganà, A. Surface adsorption of protein corona controls the cell internalization mechanism of DC-Chol−DOPE/DNA lipoplexes in serum. *Biochim. Biophys. Acta, Biomembr.* **2010**, *1798*, 536−543.
(41) Prabha, S.; Arya, G.; Chandra, R.; Ahmed, B.; Nimesh, S. Effect of Size on Biological Properties of Nanoparticles Employed in Gene Delivery. *Artif. Cells, Nanomed., Biotechnol.* **2016**, *44* (1), 83−91.
(42) Gavara, R.; Llorca, J.; Lima, J. C.; Rodríguez, L. A Luminescent Hydrogel Based on a New Au(I) Complex. *Chem. Commun.* **2013**, *49* (1), 72−74.
(43) Aguiló, E.; Gavara, R.; Baucells, C.; Guitart, M.; Lima, J. C.; Llorca, J.; Rodríguez, L. Tuning Supramolecular Aurophilic Structures: The Effect of Counterion, Positive Charge and Solvent. *Dalton Trans.* **2016**, *45* (17), 7328−7339.
(44) Svahn, N.; Sanz, I.; Rissanen, K.; Rodríguez, L. Supramolecular Assemblies and Photophysical Properties of Ionic Homo- and Heteronuclear Metallophilic Complexes. *J. Organomet. Chem.* **2019**, *897*, 170−177.
(45) Aquino, A.; Caparrós, F. J.; Aullón, G.; Ward, J. S.; Rissanen, K.; Jung, Y.; Choi, H.; Lima, J. C.; Rodríguez, L. Effect of Gold(I) on the Room-Temperature Phosphorescence of Ethynylphenanthrene. *Chem. - Eur. J.* **2021**, *27* (5), 1810−1820.
(46) de Aquino, A.; Caparrós, F. J.; Truong, K.; Rissanen, K.; Ferrer, M.; Jung, Y.; Choi, H.; Lima, J. C.; Rodríguez, L. Gold(I)-Doped Films: New Routes for Efficient Room Temperature Phosphorescent Materials. *Dalton Trans.* **2021**, *50*, 3806.
(47) Ferrer, M.; Giménez, L.; Gutiérrez, A.; Lima, J. C.; Martínez, M.; Rodríguez, L.; Martín, A.; Puttreddy, R.; Rissanen, K. Polypyridyl-Functionalizated Alkynyl Gold(I) Metallaligands Supported by Tri- and Tetradentate Phosphanes. *Dalton Trans.* **2017**, *46* (40), 13920−13934.
(48) Ca[illegible] Lima, J.; Rodríguez, L. Applications of Gold(i) Alkynyl Systems: A Growing Field to Explore. *Chem. Soc. Rev.* **2011**, *40* (11), 5442.
(49) Schmidbaur, H.; Schier, A. Aurophilic Interactions as a Subject of Current Research: An up-Date. *Chem. Soc. Rev.* **2012**, *41* (1), 370−412.
(50) Hashmi, A. S. K. Dual Gold Catalysis. *Acc. Chem. Res.* **2014**, *47* (3), 864−876.
(51) Hogarth, G.; Alvarez-Falcon, M. M. Gold(I) Alkynyl Complexes Derived from Ethynylanilines: Crystal Structure of [Au(C≡C-4-C6H4NH2){P(3-Tolyl)3}] a Polymer in the Solid State via NH···Au Contacts. *Inorg. Chim. Acta* **2005**, *358* (5), 1386−1392.
(52) Rodríguez, L.; Ferrer, M.; Crehuet, R.; Anglada, J.; Lima, J. C. Correlation between Photophysical Parameters and Gold−Gold Distances in Gold(I) (4-Pyridyl)Ethynyl Complexes. *Inorg. Chem.* **2012**, *51* (14), 7636−7641.
(53) Rejman, J.; Oberle, V.; Zuhorn, I. S.; Hoekstra, D. Size-Dependent Internalization of Particles via the Pathways of Clathrin- and Caveolae-Mediated Endocytosis. *Biochem. J.* **2004**, *377* (1), 159−169.
(54) dos Santos, T.; Varela, J.; Lynch, I.; Salvati, A.; Dawson, K. A. Effects of Transport Inhibitors on the Cellular Uptake of

https://doi.org/10.1021/acs.inorgchem.1c02359
Inorg. Chem. XXXX, XXX, XXX−XXX

Carboxylated Polystyrene Nanoparticles in Different Cell Lines. *PLoS One* **2011**, *6* (9), e24438.
(55) Chen, M.; Yi, L.; Jin, X.; Xie, Q.; Zhang, T.; Zhou, X.; Chang, H.; Fu, Y.; Zhu, J.; Zhang, Q.; Mi, M.-T. Absorption of Resveratrol by Vascular Endothelial Cells through Passive Diffusion and an SGLT1-Mediated Pathway. *J. Nutr. Biochem.* **2013**, *24* (11), 1823−1829.
(56) Stehn, J. R.; Haass, N. K.; Bonello, T.; Desouza, M.; Kottyan, G.; Treutlein, H.; Zeng, J.; Nascimento, P. R. B. B.; Sequeira, V. B.; Butler, T. L.; Allanson, M.; Fath, T.; Hill, T. A.; McCluskey, A.; Schevzov, G.; Palmer, S. J.; Hardeman, E. C.; Winlaw, D.; Reeve, V. E.; Dixon, I.; Weninger, W.; Cripe, T. P.; Gunning, P. W. A Novel Class of Anticancer Compounds Targets the Actin Cytoskeleton in Tumor Cells. *Cancer Res.* **2013**, *73* (16), 5169−5182.
(57) Foerster, F.; Braig, S.; Moser, C.; Kubisch, R.; Busse, J.; Wagner, E.; Schmoeckel, E.; Mayr, D.; Schmitt, S.; Huettel, S.; Zischka, H.; Mueller, R.; Vollmar, A. M. Targeting the Actin Cytoskeleton: Selective Antitumor Action via Trapping PKCε. *Cell Death Dis.* **2014**, *5* (8), e1398−e1398.
(58) Liu, W.; Gust, R. Update on Metal N-Heterocyclic Carbene Complexes as Potential Anti-Tumor Metallodrugs. *Coord. Chem. Rev.* **2016**, *329*, 191−213.
(59) Suarez-Huerta, N.; Mosselmans, R.; Dumont, J. E.; Robaye, B. Actin Depolymerization and Polymerization Are Required during Apoptosis in Endothelial Cells. *J. Cell. Physiol.* **2000**, *184* (2), 239−245.
(60) Huang, T. C.; Toraya, H.; Blanton, T. N.; Wu, Y. X-Ray Powder Diffraction Analysis of Silver Behenate, a Possible Low-Angle Diffraction Standard. *J. Appl. Crystallogr.* **1993**, *26* (2), 180−184.
(61) Kieffer, J.; Karkoulis, D. PyFAI, a Versatile Library for Azimuthal Regrouping. *J. Phys.: Conf. Ser.* **2013**, *425* (20), 202012.
(62) Svergun, D. I. Determination of the Regularization Parameter in Indirect-Transform Methods Using Perceptual Criteria. *J. Appl. Crystallogr.* **1992**, *25* (4), 495−503.
(63) Svergun, D. I. Restoring Low Resolution Structure of Biological Macromolecules from Solution Scattering Using Simulated Annealing. *Biophys. J.* **1999**, *76* (6), 2879−2886.
(64) Kabe, R.; Adachi, C. Organic Long Persistent Luminescence. *Nature* **2017**, *550* (7676), 384−387.
(65) Xu, J.; Takai, A.; Kobayashi, Y.; Takeuchi, M. Phosphorescence from a Pure Organic Fluorene Derivative in Solution at Room Temperature. *Chem. Commun.* **2013**, *49* (76), 8447−8449.
(66) Zhou, G.-J.; Wang, X.-Z.; Wong, W.-Y.; Yu, X.-M.; Kwok, H.-S.; Lin, Z. New Platinum(II) Complexes as Triplet Emitters for High-Efficiency Monochromatic Pure Orange Electroluminescent Devices. *J. Organomet. Chem.* **2007**, *692* (16), 3461−3473.
(67) Ferrer, M.; Mounir, M.; Rodríguez, L.; Rossell, O.; Coco, S.; Gómez-Sal, P.; Martín, A. Effect of the Organic Fragment on the Mesogenic Properties of a Series of Organogold(I) Isocyanide Complexes. X-Ray Crystal Structure of [Au(CCC5H4N)-(CNC6H4O(O)CC6H4OC10H21)]. *J. Organomet. Chem.* **2005**, *690* (9), 2200−2208.
(68) Kishpaugh, D.; Hajagos, T.; Liu, C.; Chen, Q.; Pei, Q. Applications of Fluorene Moiety Containing Polymers for Improved Scintillation Light Yield. *Nucl. Instrum. Methods Phys. Res., Sect. A* **2017**, *868* (June), 59−65.
(69) Baluja, S.; Kulshrestha, A.; Movalia, J. 1-Octanol-Water Partition Coefficient of Some Cyanopyridine and Chalcone Compounds. *Rev. Colomb. Cienc. Quim.-Farm.* **2017**, *46* (3), 342−356.
(70) Czerwińska, K.; Machura, B.; Kula, S.; Krompiec, S.; Erfurt, K.; Roma-Rodrigues, C.; Fernandes, A. R.; Shul'Pina, L. S.; Ikonnikov, N. S.; Shul'Pin, G. B. Copper(II) Complexes of Functionalized 2,2′:6′,2″-Terpyridines and 2,6-Di(Thiazol-2-Yl)Pyridine: Structure, Spectroscopy, Cytotoxicity and Catalytic Activity. *Dalton Trans.* **2017**, *46* (29), 9591−9604.
(71) Rodrigo, A. P.; Mendes, V. M.; Manadas, B.; Grosso, A. R.; Alves de Matos, A. P.; Baptista, P. V.; Costa, P. M.; Fernandes, A. R. Specific Antiproliferative Properties of Proteinaceous Toxin Secretions from the Marine Annelid Eulalia Sp. onto Ovarian Cancer Cells. *Mar. Drugs* **2021**, *19* (1), 31.

https://doi.org/10.1021/acs.inorgchem.1c02359
Inorg. Chem. XXXX, XXX, XXX−XXX